Supplemental Material can be found at:
http://www.jbc.org/content/suppl/2011/12/27/M111.325746.DC1.html

THE JOURNAL OF BIOLOGICAL CHEMISTRY VOL. 287, NO. 8, pp. 5882–5890, February 17, 2012
Published in the U.S.A.

Assembly and Architecture of Biogenesis of Lysosome-related Organelles Complex-1 (BLOC-1)*[S]

Received for publication, November 22, 2011, and in revised form, December 21, 2011 Published, JBC Papers in Press, December 27, 2011, DOI 10.1074/jbc.M111.325746

Hyung Ho Lee[‡§1], **Daniel Nemecek**[¶1], **Christina Schindler**[‖1], **William J. Smith**[‖2], **Rodolfo Ghirlando**[§], **Alasdair C. Steven**[¶3], **Juan S. Bonifacino**[‖4], **and James H. Hurley**[§5]

From the [‡]*Departments of Bio and Nano Chemistry and Integrative Biomedical Science and Engineering, Kookmin University, Seoul 136-702, Korea and the* [§]*Laboratory of Molecular Biology, NIDDK,* [¶]*NIAMS, and* [‖]*Cell Biology and Metabolism Program, Eunice Kennedy Shriver NICHD, National Institutes of Health, Bethesda, Maryland 20892*

Background: The BLOC-1 complex is critical for biogenesis of lysosome-related organelles.
Results: BLOC-1 is elongated, bends by up to 45°, and contains two heterotrimeric subcomplexes.
Conclusion: BLOC-1 is flexible hetero-octameric complex built up from two elongated heterotrimeric subcomplexes.
Significance: The length and flexibility of BLOC-1 may contribute to its interactions with membranes and SNAREs in tubular endosome biogenesis.

BLOC-1 (biogenesis of lysosome-related organelles complex-1) is critical for melanosome biogenesis and has also been implicated in neurological function and disease. We show that BLOC-1 is an elongated complex that contains one copy each of the eight subunits pallidin, Cappuccino, dysbindin, Snapin, Muted, BLOS1, BLOS2, and BLOS3. The complex appears as a linear chain of eight globular domains, ~300 Å long and ~30 Å in diameter. The individual domains are flexibly connected such that the linear chain undergoes bending by as much as 45°. Two stable subcomplexes were defined, pallidin-Cappuccino-BLOS1 and dysbindin-Snapin-BLOS2. Both subcomplexes are 1:1:1 heterotrimers that form extended structures as indicated by their hydrodynamic properties. The two subcomplexes appear to constitute flexible units within the larger BLOC-1 chain, an arrangement conducive to simultaneous interactions with multiple BLOC-1 partners in the course of tubular endosome biogenesis and sorting.

Lysosome-related organelles (LROs)[6] are present in a range of cells in multicellular eukaryotes and include lytic granules, lung lamellar bodies, platelet-dense granules, and melanosomes (1). The melanosome of the pigment cells in the skin and eye is the best studied of the LROs (1, 2). The biogenesis of the melanosome and other LROs requires the AP-3 adaptor complex, the class C Vps complex, and three BLOC (biogenesis of lysosome-related organelles complex) complexes. Components of the BLOC complexes were first discovered from the genetic analysis of the human Hermansky-Pudlak syndrome and of pigmentation phenotypes in mice (1, 2). BLOC-1, BLOC-2, and BLOC-3 contain eight, three, and two subunits, respectively (1, 2). Many of the subunits, including those of BLOC-1, contain extensive regions of predicted coiled coil. Aside from this, none of the subunits are homologous to other proteins, and they do not contain recognizable motifs predictive of function. The molecular level functions of the BLOC complexes remain one of the central unresolved issues in LRO biogenesis.

BLOC-1 contains eight subunits: dysbindin (3–6), Cappuccino (7, 8), pallidin (9–11), Muted (11), Snapin (12, 13), and BLOS1, BLOS2, and BLOS3 (13, 14). Mutation of the genes encoding the first five of these subunits leads to some of the strongest pigmentation phenotypes in mice compared with other components of the LRO biogenesis machinery. Furthermore, mutations of the genes coding for dysbindin (4), BLOS3 (15), and pallidin (16) are responsible for HPS7–9 (Hermansky-Pudlak syndrome), respectively, in humans. Variations in the same human gene coding for dysbindin, *DTNBP1*, are strongly associated with schizophrenia in some populations, suggesting that the function of dysbindin is impaired in *DTNBP1*-associated schizophrenia (17). Biochemical fractionation of dysbindin and its developmental regulation in brain suggest that dysbindin functions in neurons in its context as a subunit of BLOC-1 (18). Thus, BLOC-1 is not only a pivotal player in LRO biogenesis and HPS7–9 but may also have significance for the molecular basis for schizophrenia. In this connection, BLOC-1 is involved in the selective delivery of cargoes from cell bodies to neurites and nerve terminals (19).

The main clues to the cellular function of BLOC-1 come from electron microscopy of human melanoma cells and cells derived from mice defective in BLOC-1 genes. BLOC-1 localizes to tubular endosomes and is required for the sorting of cargo from early endosomes to melanosomes (20–22). Thus, BLOC-1 is implicated in the formation and/or maturation of

* This work was supported, in whole or in part, by the National Institutes of Health Intramural Programs of NIDDK (to J. H. H.), NICHD (to J. S. B.), and NIAMS (to A. C. S.). This work was also supported by a fellowship from the Deutsche Forschungsgemeinschaft (to C. S.).
[S] This article contains supplemental Movie S1.
[1] These authors contributed equally to this work.
[2] Present address: Merck & Co., Inc., West Point, PA 19486.
[3] To whom correspondence may be addressed: NIAMS, NIH, Bldg. 50, Rm. 1517, Bethesda, MD 20892-8025. Tel.: 301-496-0132; E-mail: stevena@mail.nih.gov.
[4] To whom correspondence may be addressed: NICHD, NIH, Bldg. 18T, Rm. 101, Bethesda, MD 20892. Tel.: 301-496-6368; Fax: 301-402-0078; E-mail: juan@helix.nih.gov.
[5] To whom correspondence may be addressed: NIDDK, NIH, Bldg. 50, Rm. 4517, Bethesda, MD 20892-0580. Tel.: 301-402-4703; Fax: 301-480-0639; E-mail: hurley@helix.nih.gov.
[6] The abbreviations used are: LRO, lysosome-related organelle; TEV, tobacco etch virus; Ni-NTA, nickel-nitrilotriacetic acid.

Downloaded from www.jbc.org at National Institutes of Health Library, on July 12, 2012

tubular vesicular intermediates between endosomes and LROs. Potential clues to the molecular function of BLOC-1 come from the identification of a great many interaction partners for individual subunits of BLOC-1 (23). The number of well validated partners for the intact BLOC-1 complex is much smaller and includes the AP-3 adaptor complex (20, 21), the SNARES syntaxin-13 and SNAP-25 and their close relatives (6), the WASH complex (which promotes actin nucleation) (24), and a K*x*DL-containing protein (25).

To make progress in understanding the molecular level function of BLOC-1, it will be critical to understand the spatial organization and relative locations of the interaction sites with AP-3, SNAREs, and other partners. The complexity of BLOC-1, with eight subunits, makes it a daunting target for structural analysis. As a first step in the mechanistic and structural dissection of this complex, we generated a recombinant version of the hetero-octamer and characterized it by analytical ultracentrifugation and negative stain electron microscopy. We found that BLOC-1 is an elongated flexible molecule with apparently eight domains and with one copy of each subunit. We also found that the trio pallidin, Cappuccino, and BLOS1 and another trio, dysbindin, Snapin, and BLOS2, form elongated subcomplexes of 1:1:1 stoichiometry. The regions of these six subunits responsible for core interactions in the subcomplexes were mapped. Taking these data together with modeling of the coiled coils and hydrodynamic analysis, we developed a low resolution model of the architecture of the core of BLOC-1.

EXPERIMENTAL PROCEDURES

Expression and Purification of the Complete BLOC-1 Complex—DNAs coding for human pallidin and dysbindin were amplified by PCR, and the human forms of Snapin, Cappuccino, Muted, BLOS1, BLOS2, and BLOS3 were synthesized by PCR-based gene synthesis. Oligonucleotides were designed by the program DNAWorks (26). BLOC-1 subunits were generated containing the Shine-Dalgarno translational start signal and subcloned sequentially into a modified polycistronic pST39 vector (27). His_6 and GST tags with tobacco etch virus (TEV) protease cleavage sites were attached to the N terminus of pallidin and the C terminus of dysbindin, respectively (see Fig. 1*B*). Constructs of the BLOC-1 complex were expressed in *Escherichia coli* BL21 Star(DE3) cells (Invitrogen) grown in LB medium (Sigma) and induced with 0.2 mM isopropyl β-D-thiogalactopyranoside at $A_{600} = 0.6$. Cultures were grown at 20 °C for 14 h after induction. Cells were lysed by sonication in 50 mM Tris (pH 7.4), 300 mM NaCl, and 5 mM β-mercaptoethanol supplemented with 100 μl of protease inhibitor mixture (Sigma)/liter of culture medium. BLOC-1 was isolated from the lysate using glutathione resin (GE Healthcare). For removal of His_6 and GST tags on pallidin and dysbindin, respectively, TEV protease was used in conjunction with dialysis against 50 mM Tris (pH 7.4), 300 mM NaCl, and 5 mM β-mercaptoethanol. Histidine-tagged TEV protease was removed from the protein sample by a second pass over a nickel-nitrilotriacetic acid (Ni-NTA) column. Recombinant BLOC-1 was purified by size exclusion chromatography on a Superose 6 column in 0.4 M NaCl, 0.05 M Tris (pH 8.5), 1 mM EDTA, 1 mM tris(2-carboxyethyl)phosphine, and 5% (v/v) glycerol.

Pulldown Experiments—Cells were lysed in 50 mM Tris (pH 7.4), 150 mM NaCl, 1 mM EDTA, 0.5% Triton X-100, 10% glycerol, and 1× protease inhibitor mixture (Sigma). The lysate was cleared by centrifugation for 15 min at 20,000 × *g*. For each sample, 500 μg of total protein (as determined by BCA assay) from the cell lysate was brought to a volume of 1 ml and was further cleared by incubation with 5 μg of GST and 20 μl of glutathione-Sepharose beads (GE Healthcare) for 1 h at 4 °C. The beads were removed by brief centrifugation, and 1 ml of supernatant was incubated with 20 μl of fresh glutathione-Sepharose beads loaded with GST or GST-BLOC-1 for 1 h at 4 °C. After three washes in the lysis buffer, bound proteins were recovered by boiling the beads in sample buffer. Bound proteins were resolved by SDS-PAGE and analyzed by immunoblotting with anti-AP-3σ3 and AP-3β3 antibodies (28, 29) and anti-AP-3δ antibody (specific for human AP-3δ; BD Biosciences).

Expression and Purification of BLOC-1 Subcomplexes—For pallidin-Cappuccino-BLOS1 complexes, DNA sequences encoding human pallidin (amino acids 1–172, 33–172, 33–160, 33–140, and 45–125), Cappuccino (amino acids 1–177, 75–177, and 82–177), and BLOS1 (amino acids 1–125, 51–125, and 60–125) were amplified by PCR from the pST39 vector containing BLOC-1 (see Fig. 1*A*). The products of pallidin and Cappuccino were inserted into the pGST2 vector (30), and the product of BLOS1 was cloned into the pRSFDuet-1 vector (Novagen). The construct for the Cappuccino subunit was generated with a Shine-Dalgarno translational start signal. GST and His_6 tags with TEV protease cleavage sites were attached to the N termini of pallidin and BLOS1, respectively. The plasmids were cotransformed into *E. coli* BL21 Star(DE3) cells, and the protein was expressed at 20 °C for 15 h by induction with 0.3 mM isopropyl β-D-thiogalactopyranoside when the cells reached $A_{600} = 0.6$. Cells were lysed by sonication in 20 mM Tris (pH 8.0) and 500 mM NaCl (buffer A) and centrifuged. The supernatant was applied to a glutathione-Sepharose column (GE Healthcare). The protein was eluted with buffer A containing 15 mM reduced glutathione and was applied to a Ni-NTA column. The protein eluted with buffer A containing 500 mM imidazole was cleaved overnight with His_6-tagged TEV protease at 4 °C. The protein was further purified by size exclusion chromatography (Superdex 200 16/60). Fractions were pooled and concentrated to 3 mg/ml in 20 mM Tris (pH 8.0) and 200 mM NaCl.

For the pallidin-BLOS1 and pallidin-Cappuccino complexes, the plasmids containing the corresponding sequences were cotransformed into *E. coli* BL21 Star(DE3) cells and purified as described above. For the dysbindin-Snapin-BLOS2 complex, DNA sequences encoding human dysbindin (amino acids 1–217 and 48–140), Snapin (amino acids 1–136), and BLOS2 (amino acids 1–142) were amplified using PCR. The products of BLOS2 and Snapin were inserted into the pRSFDuet-1 vector, and the product of dysbindin was cloned into the pGST2 vector (30). A GST tag with a TEV protease cleavage site and a hexahistidine tag were fused to the N termini of dysbindin and BLOS2, respectively. The plasmids were cotransformed into *E. coli* BL21 Star(DE3) cells, and the protein was purified as described above.

Downloaded from www.jbc.org at National Institutes of Health Library, on July 12, 2012

Limited Proteolysis—The pallidin(33–160)-Cappuccino(1–177)-BLOS1(51–125) complex (1 mg/ml) was digested with endoproteinase Glu-C (0.03 μg/μl; New England Biolabs) at 22 °C. The reaction buffer contained 15 mM Tris (pH 8.0), 0.15 mM Glu-Glu, and 100 mM NaCl. The digested protein samples were separated on SDS-polyacrylamide gel, transferred to polyvinylidene fluoride membrane, and stained with SimplyBlue SafeStain (Invitrogen). Bands were excised and subjected to N-terminal amino acid sequencing using a 492 cLC protein sequencer (Applied Biosystems). Limited proteolysis was also combined with size exclusion chromatography to isolate and identify the core of the pallidin(33–160)-Cappuccino(1–177)-BLOS1(51–125) complex. Proteolyzed samples of pallidin(33–160)-Cappuccino(1–177)-BLOS1(51–125) were fractionated by passing them over a Superdex 200 10/300 column (GE Healthcare). The resulting size exclusion chromatography fractions were further separated by SDS-PAGE and subsequently sequenced. In some cases, mass spectrometry (MALDI-TOF) analysis was utilized to confirm the identity of the proteins in the associated subcomplex. MALDI-TOF samples were prepared by mixing 1 μl of protein sample in 49 μl of matrix buffer (0.07% trifluoroacetic acid and 33% acetonitrile). A matrix solution was prepared by mixing excess sinapinic acid with 30 μl of matrix buffer. 1 μl of each sample solution and matrix solution was spotted on a gold plate and dried at room temperature. The plated samples were then analyzed on a Voyager-DE MALDI-TOF mass spectrometer (Applied Biosystems).

Analytical Ultracentrifugation—Sedimentation velocity experiments were conducted at 20.0 °C on a Beckman Coulter ProteomeLab XL-I analytical ultracentrifuge. Samples of BLOC-1 (loading volume of 400 μl, 12-mm two-channel centerpiece cells) were analyzed in separate experiments at loading concentrations ranging from 2.6 to 11.2 μM and a rotor speed of 50 krpm. 80 absorbance scans at 4.3- or 5.3-min intervals were collected as single measurements at 280 nm using a radial spacing of 0.003 cm. Experiments were carried out in 0.4 M NaCl, 0.05 M Tris (pH 8.5), 1 mM EDTA, 1 mM tris(2-carboxyethyl)-phosphine, and 5% (v/v) glycerol, and buffer exchange was achieved by size exclusion chromatography over a Superose 6 column. Data were analyzed by SEDFIT 11.71 (31) in terms of a continuous $c(s)$ distribution covering an s range of 0.0–10.0 S with a resolution of 100 and a confidence level (F ratio) of 0.68. Excellent fits were obtained with root mean square deviations of 0.0040–0.0071 absorbance units. Solution densities (ρ) were measured at 20.00 °C on a Mettler Toledo DE51 density meter, and solution viscosities (η) were measured at 20.00 °C using an Anton-Paar AMVn rolling ball viscometer. The partial specific volume (ν) was calculated based on the amino acid composition using SEDNTERP 1.09 (32).

Size Exclusion Chromatography with Multiangle Light Scattering—These experiments were performed using an Agilent 1200 HPLC system coupled to a Wyatt DAWN HELEOS II multiangle light scattering instrument and a Wyatt Optilab rEX differential refractometer. For chromatographic separation, a TSKgel G4000SW size exclusion column (Tosoh Bioscience) with a 20-μl sample loop was used at a flow rate of 0.4 ml/min in the same running buffer (20 mM Tris (pH 8.0) and 200 mM NaCl). The outputs were analyzed using ASTRA V software (Wyatt). Multi-angle light scattering signals, combined with the protein concentration determined by refractive index, were used to calculate the molecular mass of the complex. Quasi-elastic light scattering data were collected using the HELEOS II instrument simultaneously to measure the hydrodynamic radius of the pallidin(33–160)-Cappuccino(1–177)-BLOS1(51–125) complex.

Negative Stain Electron Microscopy—The BLOC-1 sample was diluted to ~15 μg/ml in 50 mM Tris (pH 8.0) and 200 mM NaCl, adsorbed onto a thin carbon film according to the method of Valentine and Green (33), and negatively stained with fresh 2% uranyl formate. The stained specimens were imaged on a Philips CM120 electron microscope operating at 120 kV. Micrographs were recorded at magnification of ×60,000.

Image Processing—Micrographs were digitized using a Nikon Super COOLSCAN 9000 ED at 4000 dots/inch (1.16 Å/pixel). About 2000 particles were picked and extracted in bshow, binned, and contrast transfer function-corrected by phase flipping using bint and bctf of the Bsoft package (34). Alignment and classification of the two-dimensional single particles were done in the SPIDER package (35). Initially, all particles were pre-aligned into a vertical orientation using a reference-free alignment algorithm as implemented in SPIDER (36). Further iterations of alignments and classifications consisted of two steps. First, the aligned particles were classified using Ward's clustering and hierarchical ascendant classification. Individual classes were selected according to the clustering dendrogram and quality of the class averages. Each class had a well defined shape of the class average, and further splitting of the class led to the same class averages. Second, class averages of the selected classes were used as references in several rounds of multi-reference alignments and mutually exclusive classification according to cross-correlation coefficients from the multi-reference alignments. These two steps of classification and averaging were repeated in several iterations until the solution converged to stable class averages. A tight soft mask derived from the variance map of the class averages was used in the later iterations. The final class averages were selected after the hierarchical ascendant classification, aligned to a relatively straight top part of the molecule, and ordered according to curvature of the bottom part.

RESULTS

Recombinant BLOC-1 Is a Stable Hetero-octamer—All eight subunits of BLOC-1 were coexpressed from a single polycistronic plasmid in *E. coli* (Fig. 1*A*). A GST tag was placed at the C terminus of dysbindin and used to isolate the complex by glutathione-Sepharose affinity chromatography. All eight subunits co-purified on affinity and Superose 6 chromatography, demonstrating assembly of a stable recombinant complex (Fig. 1*B*). The chromatography peak corresponded to a Stokes radius (R_H) of 8.6 nm. This value is similar to those of 9.4–9.5 nm obtained for BLOC-1 in cell lysates (6, 13) and 8.9 nm obtained for BLOC-1 in bovine liver cytosol (11).

BLOC-1 Has an Elongated Structure and a 1:1:1:1:1:1:1:1 Subunit Stoichiometry—Sedimentation velocity experiments on different preparations of BLOC-1 showed the presence of a major species accounting for at least 95% of the loading absorbance (Fig. 1*C*). This species has a sedimentation coefficient

Downloaded from www.jbc.org at National Institutes of Health Library, on July 12, 2012

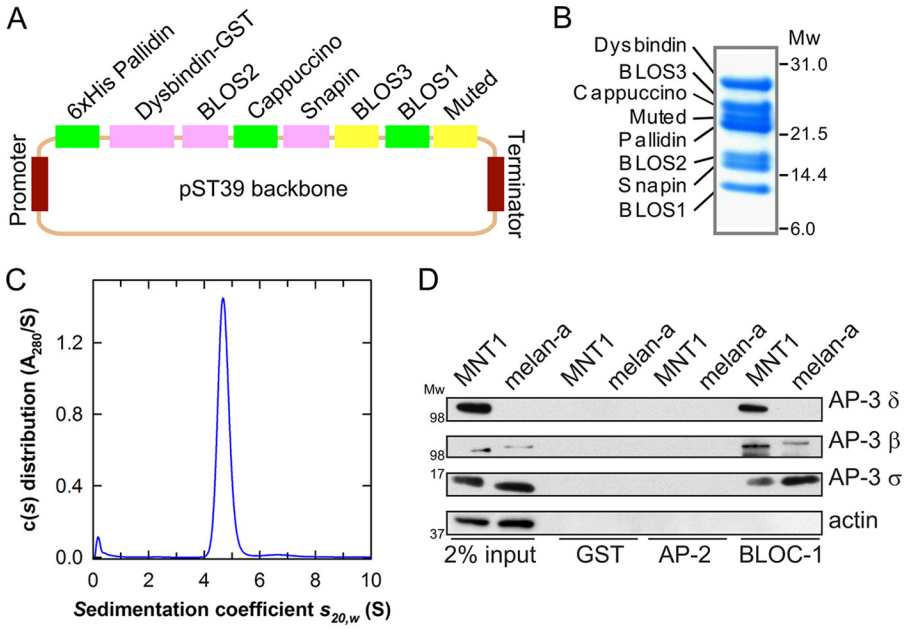

FIGURE 1. **Assembly and purification of the complete BLOC-1 complex.** *A*, schematic of the polycistronic expression cassettes used for the expression and purification of recombinant BLOC-1 in pST39. *B*, Coomassie Blue gel of BLOC-1 consisting of pallidin, dysbindin(1–217,) BLOS2, Cappuccino, Snapin, BLOS3, BLOS1, and Muted subunits. *C*, analytical ultracentrifugation of the full BLOC-1 complex at 5.3 μM. *D*, a lysate of human MNT1 and mouse melan-a melanoma cells was applied to GST, GST-AP-2 core, and GST-BLOC-1 immobilized on glutathione-Sepharose. After washing, the bound proteins were analyzed by SDS-PAGE and immunoblotting using the antibodies indicated. 2% of the input is shown.

($s_{20,w}$) of 4.75 ± 0.04 S, which is similar to that determined for the native complex (10). Based on the calculated mass of the complex, this corresponds to $R_H = 8.2 \pm 0.1$ nm, in good agreement with the result from size exclusion chromatography. The $c(s)$ analyses also returned an average frictional ratio (f/f_o) of 1.93 ± 0.03, consistent with an asymmetric rod-like species. Based on this frictional ratio, a molecular mass of 128 ± 3 kDa was determined; even though this value is lower that that calculated for the recombinant complex (162.5 kDa), analysis by SDS-PAGE post-centrifugation showed that all of the individual components are present. It should be noted that interference data were also collected for the BLOC-1 sample at 2.6 μM: the major species observed in the $c(s)$ analysis (root mean square deviation = 0.0073 fringes) has an $s_{20,w}$ of 4.69 S; based on the experimental f/f_o of 2.26, a molecular mass of 159 kDa was determined.

Recombinant BLOC-1 Binds to AP-3—To determine whether purified recombinant BLOC-1 is functional, its ability to pull down endogenous AP-3 (20) from MNT1 and melan-a melanocytic cell lines (37, 38) was tested. BLOC-1 pulled down AP-3 from both cell lines as assessed by immunoblotting against the β3 and σ3 subunits and from MNT1 cells as additionally determined by immunoblotting against the δ subunit (Fig. 1*D*). No immunoreactivity was observed when either GST or GST-AP-2 (39) was used as a negative control. These data indicate that the recombinant BLOC-1 sample used in the structural studies that follow is functionally competent for a well characterized biochemical property of the endogenous complex, binding to AP-3.

BLOC-1 Is a Linear Chain of Eight Flexibly Connected Domains—Dispersions of individual BLOC-1 complexes were visualized by negative stain electron microscopy (Fig. 2*A*). Because the complex is highly elongated, the molecules deposit on the grid so as to present almost exclusively side views. To enhance the images, class averaging was performed (Fig. 2*B*,

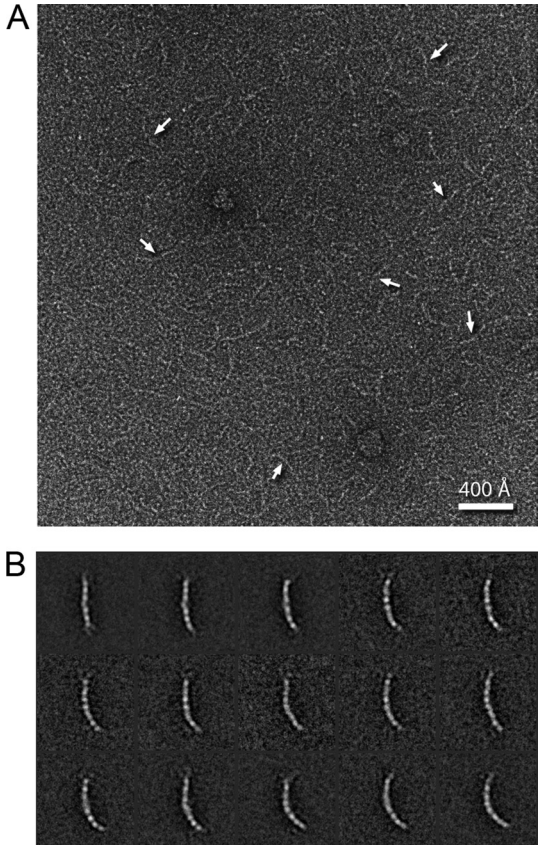

FIGURE 2. **Structure and flexibility of the BLOC-1 molecule.** *A*, negative stain electron micrograph of BLOC-1 molecules (*white arrows*) negatively stained with uranyl formate using the method of Valentine and Green (33). *B*, class averages of BLOC-1 molecules ordered from *top left* to *bottom right* according to their curvature. The averages were obtained in several iterations of multivariate statistical analysis and multi-reference classification. Statistics and dimensions of the class averages are summarized in Table 1.

Downloaded from www.jbc.org at National Institutes of Health Library, on July 12, 2012

TABLE 1
Analysis of BLOC-1 class averages from negative stain electron microscopy

	Class														
	1	2	3	4	5	6	7	8	9	10	11	12	13	14	15
Curvature	173°	160°	160°	159°	153°	147°	147°	148°	148°	154°	149°	146°	139°	139°	135°
Length (Å)	262	271	266	261	266	286	290	291	293	305	303	299	296	300	292
No. particles	177	232	198	83	69	79	96	45	65	91	115	114	139	93	105
$FRC_{0.5}$ (Å)	27	28	28	29	29	29	29	30	29	28	29	28	27	29	28

Table 1, and supplemental Movie S1). The class averages depict BLOC-1 as consisting of eight globular domains of approximately equal diameter (~30 Å) connected in a linear chain. The variety of shapes seen in the class averages indicate that BLOC-1 has a flexible structure, with at least one bend point near the middle of the molecule.

The majority of class averages shows eight well defined domains with a contour length of 294 ± 5 Å. A few classes are somewhat shorter, 265 ± 5 Å, and show seven globular domains. We interpret the majority eight-domain species as the intact complex. The seven-domain species may have shed a subunit at some stage of the isolation procedure or preparation for EM, although, in this context, we do not equate each of the eight domains visualized with a different subunit (see below). An alternative explanation for the class averages with seven globular domains is that a terminal domain has become disorganized and consequently poorly visualized (see diffuse density at end of top left class average in Fig. 2*B*).

Identification of the Pallidin-Cappuccino-BLOS1 Subcomplex—In an effort originally intended to engineer a more stable and soluble form of BLOC-1 for structural studies, a predicted unfolded region at the C terminus of Cappuccino was deleted, leaving the C-terminal boundary at residue 177. This complex was initially purified by Ni-NTA chromatography using a hexahistidine tag fused to the N terminus of pallidin in this construct. When the eluate from this step was applied to a size exclusion chromatography column, it was separated into two major peaks (Fig. 3*A*). The most prominent of these peaks corresponded to the BLOC-1 octamer as seen following glutathione affinity purification (Fig. 3*A*, highlighted by *dashed lines*). This was followed by a peak corresponding to a Stokes radius of 4.8 nm that contained three bands visible on SDS-PAGE (Fig. 3*A*, *dashed lines*). The bands in the second peak were analyzed by automated Edman degradation and found to correspond to pallidin, Cappuccino, and BLOS1 (Fig. 3*B*).

Identification of the Dysbindin-Snapin-BLOS2 Subcomplex—Having defined the pallidin-Cappuccino-BLOS1 trio as a discrete subcomplex, we sought to determine whether some or all of the remaining five subunits form another stable subcomplex. A truncated form of dysbindin was used as a bait to test the hypothesis that such a complex exists. Dysbindin was truncated to its predicted coiled-coil core, residues 47–140, and fused to an N-terminal GST tag (Fig. 4*A*). This construct was coexpressed with Cappuccino, Snapin, Muted, BLOS2, and BLOS3. Pallidin and BLOS1 were intentionally omitted in this experiment to prevent formation of the full complex and the pallidin-Cappuccino-BLOS1 subcomplex. Cappuccino was included in the experiment primarily due to the convenience in deriving the construct from the hetero-octamer expression plasmid, but its presence also served as a control for the specificity of subcomplex formation. GST-dysbindin co-purified with stoichiometric amounts of Snapin and BLOS2, but there was no evidence for the presence of Cappuccino, Muted, or BLOS3 (Fig. 4*B*). Following removal of the GST tag, the dysbindin-Snapin-BLOS2 subcomplex eluted at a volume corresponding to a Stokes radius of 5.3 nm (Fig. 4*C*). Given the calculated molecular mass of 41.8 kDa for this construct, a Stokes radius of ~2.6 nm would have been expected for a hydrated globular protein of the same molecular mass. The actual value of 5.3 nm indicates that the complex is highly elongated.

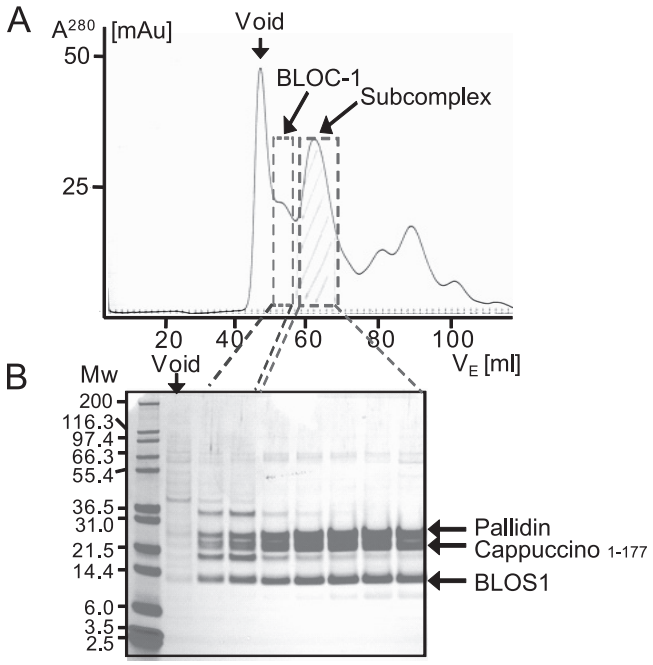

FIGURE 3. **Identification of the pallidin-Cappuccino-BLOS1 subcomplex.** *A*, size exclusion chromatography profile of His_6-pallidin-Cappuccino(1–177) variant BLOC-1 following initial purification by Ni-NTA chromatography. *mAu*, milli-absorbance units. *B*, Coomassie Blue gel of the BLOC-1 complex and subcomplex isolated in *A*. *Arrows* indicate pallidin, Cappuccino(1–177), and BLOS1, respectively. Bands were excised and subjected to N-terminal amino acid sequencing to confirm each subunit.

Pallidin-Cappuccino-BLOS1 Subcomplex Contains a Proteolytically Stable Core—The pallidin-Cappuccino-BLOS1 subcomplex was subjected to limited proteolysis by Glu-C (Fig. 5*A*), and the fragments were separated by size exclusion chromatography (Fig. 5*B*). The main peak contained three bands, which were sequenced and shown to correspond to residue 33 of pallidin, residue 82 of Cappuccino, and residue 60 of BLOS1. The C-terminal boundaries of the fragments were inferred on the basis of MALDI-TOF mass spectra and the locations of potential Glu-C sites. The stable core contained all of the predicted coiled-coil region of Cappuccino, all but the N- and C-terminal 32–33 residues of pallidin, and the C-terminal half of BLOS1 (Fig. 5*C*).

Downloaded from www.jbc.org at National Institutes of Health Library, on July 12, 2012

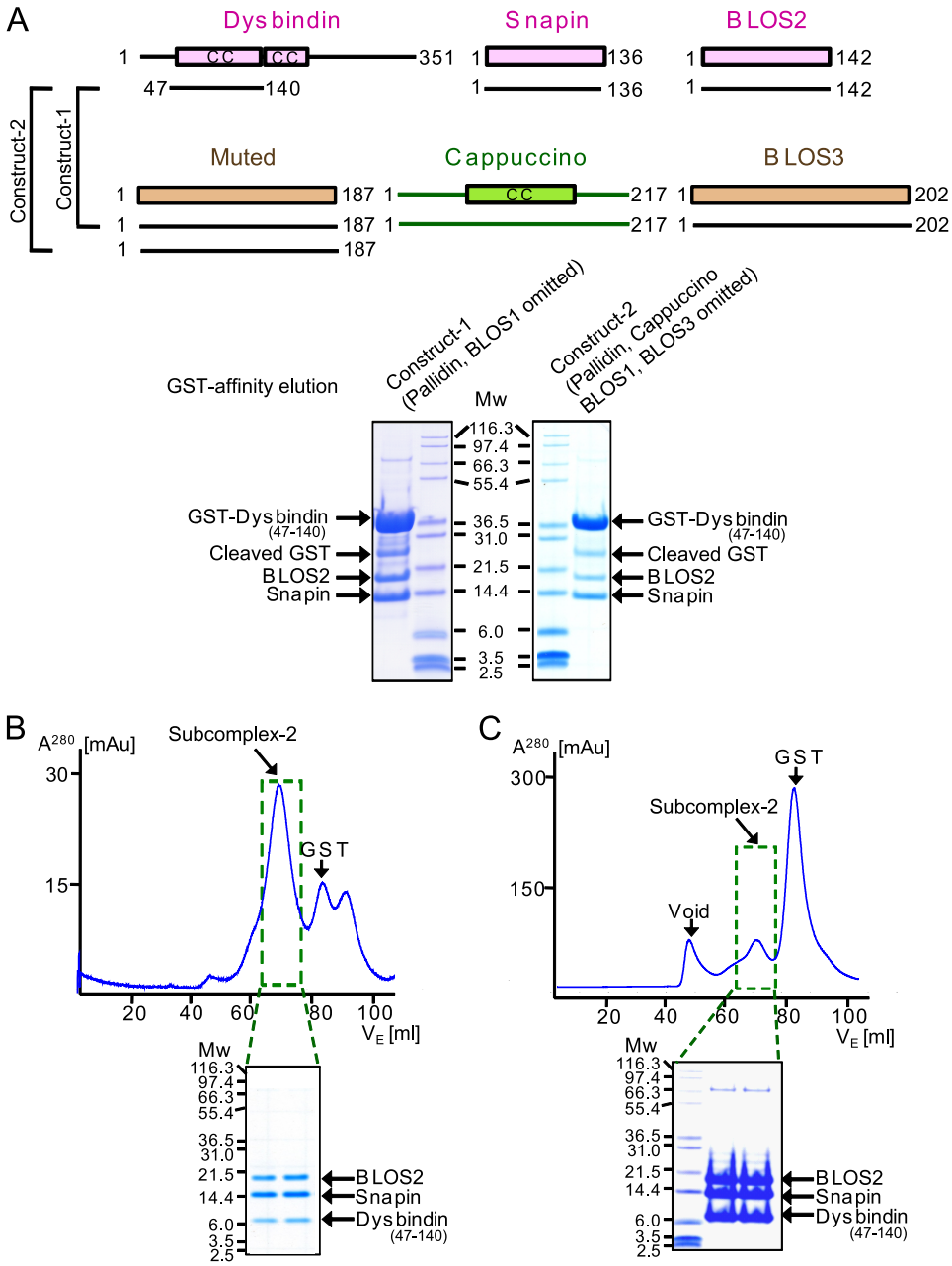

FIGURE 4. **Dysbindin-Snapin-BLOS2 subcomplex.** *A*, constructs used to identify the core of the dysbindin-Snapin-BLOS2 subcomplex. *CC*, coiled coil. *B*, Coomassie Blue gel of the BLOC-1 subcomplex isolated by size exclusion chromatography of the GST-dysbindin-Cappuccino(1–177) variant of the complex. *mAu*, milli-absorbance units. *C*, size exclusion chromatography profile of the recombinant dysbindin(47–140)-Snapin-BLOS2 complex and Coomassie Blue gel.

Hydrodynamics of the Pallidin-Cappuccino-BLOS1 Subcomplex—The subcomplex was analyzed by light scattering to determine its mass and Stokes radius. The pallidin(33–160)-Cappuccino(1–177)-BLOS1(51–125) subcomplex was found to have a mass of 43.2 kDa and a Stokes radius of 4.6 nm (Fig. 6*A*). The sum of the masses of the subunits is 42.8 kDa, so the light scattering experiment is consistent with a 1:1:1 stoichiometry in the subcomplex. The Stokes radius of 4.6 nm for a subcomplex of this size (compared with the expected value of ~2.6 nm for a hydrated globular 43-kDa protein) indicates that it is highly elongated. The dysbindin-Snapin-BLOS2 complex exhibited heterogeneity by light scattering, and accurate values of these parameters could not be obtained by this method. The value of 5.3 nm obtained for this complex by size exclusion chromatography does indicate, however, that this subcomplex is also elongated.

Coiled-coil Prediction—The sequences of the six subunits identified as belonging to stable subcomplexes were analyzed using MULTICOIL (40) to identify whether the coiled coils were most likely to be dimeric or trimeric. In all cases, a preference for a trimeric coiled coil was predicted, ranging from 1.4-fold for BLOS2 to almost 9-fold for Snapin (Fig. 7*A*).

DISCUSSION

Here, we have shown that BLOC-1 assembly can be reconstituted in a bacterial expression system and that the recombi-

Downloaded from www.jbc.org at National Institutes of Health Library, on July 12, 2012

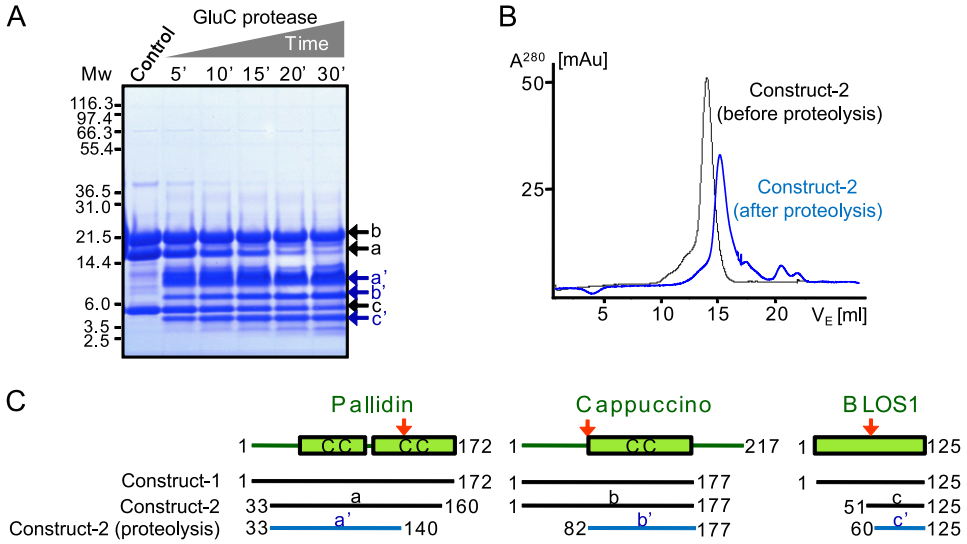

FIGURE 5. **Mapping the stable core of the pallidin-Cappuccino-BLOS1 subcomplex.** *A*, limited proteolysis of the His_6-pallidin-Cappuccino(1–177)-BLOS1 subcomplex. *B*, size exclusion chromatography of the intact and Glu-C-treated (30 min) subcomplexes. Cleaved products were confirmed by N-terminal amino acid sequencing and mass spectrometry (MALDI-TOF). *mAu*, milli-absorbance units. *C*, constructs designed on the basis of boundaries from limited proteolysis. *CC*, coiled coil.

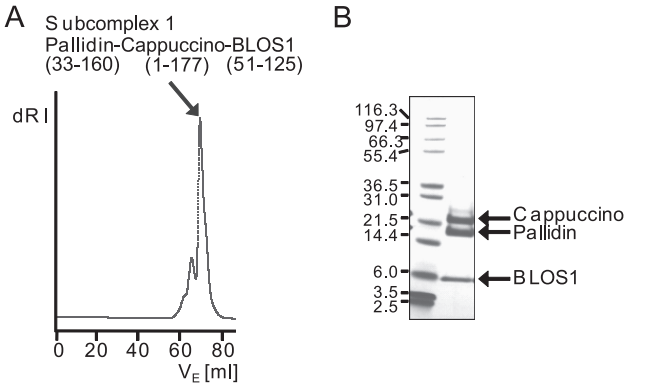

C

	Method	Expected molecular mass (kDa)	Obtained molecular mass (kDa)	R_H (nm)	Stoichiometry
Subcomplex 1	SLS	4.28×10^4	4.32×10^4	4.6	1:1:1

FIGURE 6. **Hydrodynamic analysis of core the pallidin-Cappuccino-BLOS1 subcomplex.** *A*, size exclusion chromatography of the pallidin(33–160)-Cappuccino(1–177)-BLOS1(51–125) subcomplex using a TSKgel G4000SW size exclusion column. *B*, Coomassie Blue-stained gel of the pallidin(33–160)-Cappuccino(1–177)-BLOS1(51–125) subcomplex. *C*, summary of hydrodynamic analysis. *dRI*, differential refractive index.

nant complex behaves hydrodynamically like the complex isolated from cells (10, 13). We have examined the robustness of intra-BLOC-1 interactions to various perturbations, including alternative tags, trimming the boundaries of recombinant constructs, limited proteolysis, and the deliberate omission of selected subunits. These tests resulted in the identification of two stable heterotrimeric subcomplexes that appear to form the structural core of the complex.

For the first time, we have an overall view of how the subunits are organized within BLOC-1. The complex consists of eight globular domains that are flexibly connected into a linear chain, ~300 Å in length and 30 Å in diameter. This organization results in flexible bending of the complex approximately in the center of the molecule. The hydrodynamic analysis also indicates that the complex is elongated, with the heterotrimeric subcomplexes forming separate arms. A compact parallel arrangement of the heterotrimers would not be consistent with the high value for the Stokes radius of the overall complex.

In combination with previous analysis by yeast two-hybrid methods (13), the hierarchical organization of BLOC-1 can be modeled. The strong association of the subunits of the two heterotrimers with each other makes it unlikely that the eight domains of BLOC-1 correspond directly to individual subunits, although this remains a possibility. The scheme illustrated in Fig. 7*B* presents one way to reconcile the presence of eight globular domains in a complex formed from eight subunits but just two tight subcomplexes. The predicted trimeric coiled-coil character of much of the subunit sequences is taken into consideration in this scheme.

Most of the intra-subcomplex interactions were also seen in the yeast two-hybrid analysis (13), including the interactions of pallidin with both Cappuccino and BLOS1 and the interaction of Snapin with both dysbindin and BLOS2. Several other interactions suggest how the two subcomplexes could be joined by multiple interactions to form the full complex. The pairs dysbindin-pallidin and Cappuccino-Snapin interact in yeast two-hybrid analysis. BLOS1 and BLOS2 interact with one another, as do Snapin and Cappuccino. Muted and BLOS3 appear to be more peripherally associated in that they are the first to be shed from the full complex when it is exposed to perturbations. Indeed, a six-subunit cognate of the BLOC-1 complex was recently discovered in yeast (25). This complex contains clear orthologs of the core subunits BLOS1, Snapin, and Cappuccino, but it is not clear if any of the remaining three subunits correspond to Muted or BLOS3. Muted and BLOS3 have a smaller number of interactions with the rest of the complex than any other subunits, and these interactions are formed exclusively with the dysbindin-Snapin-BLOS2 heterotrimer. These interactions are likely mediated at least in part by non-core portions of dysbindin and will be important to pursue in future biochem-

Downloaded from www.jbc.org at National Institutes of Health Library, on July 12, 2012

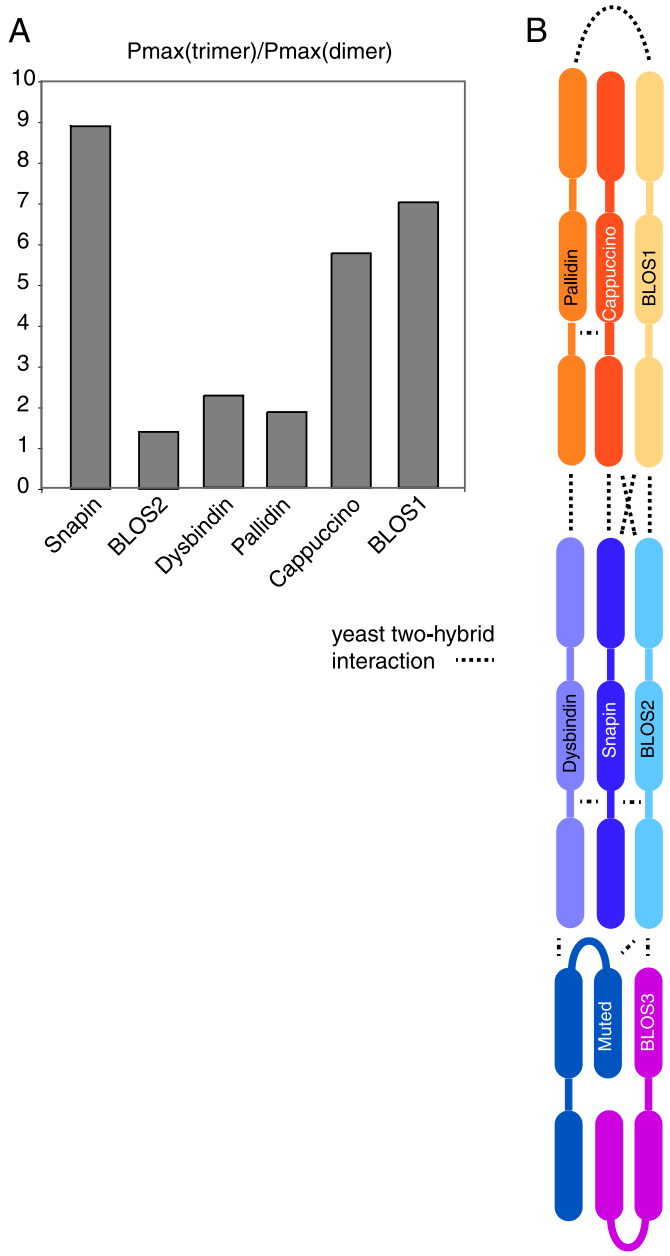

FIGURE 7. **Model for BLOC-1 organization.** *A*, MULTICOIL (40) was used to assess the relative probability of dimeric *versus* trimeric coiled coils. This method is not preferred for assessing the absolute probability of coiled-coil conformation or for predicting the boundaries of coiled coils, so only the ratios of *P*(trimer) *versus* *P*(dimer) are shown. The maximum probability as a function of residue number was used. *B*, model for the arrangement of the subcomplexes identified in this study as shown and compared with the interactions reported from yeast two-hybrid mapping (13).

ical analysis. Significantly, the binding sites for the two classes of SNARE ligands, syntaxin-13-like (10) and SNAP-25-like (5, 12, 13, 41), map to the two different heterotrimeric components of the complex.

With further structural analysis, even at low resolution, it should be possible to determine the relative positions of the syntaxin-13- and SNAP-25-binding sites. An analysis of the locations of SNARE-binding sites on the Golgi-tethering complex Dsl1 (42) illustrates how placement of these sites on a structure can shed light on the molecular function of the complex. The data herein bring us a step closer to understanding the molecular function of BLOC-1 in LRO biogenesis and neurobiology.

Acknowledgments—We thank Xuefeng Ren for help with light scattering and Daniel Kloer for assistance with purification of the intact BLOC-1 complex.

REFERENCES

1. Dell'Angelica, E. C. (2004) The building BLOC(k)s of lysosomes and related organelles. *Curr. Opin. Cell Biol.* **16,** 458–464
2. Raposo, G., and Marks, M. S. (2007) Melanosomes–dark organelles enlighten endosomal membrane transport. *Nat. Rev. Mol. Cell Biol.* **8,** 786–797
3. Benson, M. A., Newey, S. E., Martin-Rendon, E., Hawkes, R., and Blake, D. J. (2001) Dysbindin, a novel coiled coil-containing protein that interacts with the dystrobrevins in muscle and brain. *J. Biol. Chem.* **276,** 24232–24241
4. Li, W., Zhang, Q., Oiso, N., Novak, E. K., Gautam, R., O'Brien, E. P., Tinsley, C. L., Blake, D. J., Spritz, R. A., Copeland, N. G., Jenkins, N. A., Amato, D., Roe, B. A., Starcevic, M., Dell'Angelica, E. C., Elliott, R. W., Mishra, V., Kingsmore, S. F., Paylor, R. E., and Swank, R. T. (2003) Hermansky-Pudlak syndrome type 7 (HPS7) results from mutant dysbindin, a member of the biogenesis of lysosome-related organelles complex-1 (BLOC-1). *Nat. Genet.* **35,** 84–89
5. Talbot, K., Cho, D. S., Ong, W. Y., Benson, M. A., Han, L. Y., Kazi, H. A., Kamins, J., Hahn, C. G., Blake, D. J., and Arnold, S. E. (2006) Dysbindin-1 is a synaptic and microtubular protein that binds brain Snapin. *Hum. Mol. Genet.* **15,** 3041–3054
6. Ghiani, C. A., Starcevic, M., Rodriguez-Fernandez, I. A., Nazarian, R., Cheli, V. T., Chan, L. N., Malvar, J. S., de Vellis, J., Sabattia, C., and Dell'Angelica, E. C. (2009) The dysbindin-containing complex (BLOC-1) in brain. Developmental regulation, interaction with SNARE proteins, and role in neurite outgrowth. *Mol. Psychiatry* **115,** 204–215
7. Gwynn, B., Ciciotte, S. L., Hunter, S. J., Washburn, L. L., Smith, R. S., Andersen, S. G., Swank, R. T., Dell'Angelica, E. C., Bonifacino, J. S., Eicher, E. M., and Peters, L. L. (2000) Defects in the cappuccino (*cno*) gene on mouse chromosome 5 and human 4p cause Hermansky-Pudlak syndrome by an AP-3-independent mechanism. *Blood* **96,** 4227–4235
8. Ciciotte, S. L., Gwynn, B., Moriyama, K., Huizing, M., Gahl, W. A., Bonifacino, J. S., and Peters, L. L. (2003) Cappuccino, a mouse model of Hermansky-Pudlak syndrome, encodes a novel protein that is part of the pallidin-muted complex (BLOC-1). *Blood* **101,** 4402–4407
9. Huang, L., Kuo, Y. M., and Gitschier, J. (1999) The pallid gene encodes a novel, syntaxin 13-interacting protein involved in platelet storage pool deficiency. *Nat. Genet.* **23,** 329–332
10. Moriyama, K., and Bonifacino, J. S. (2002) Pallidin is a component of a multiprotein complex involved in the biogenesis of lysosome-related organelles. *Traffic* **3,** 666–677
11. Falcón-Pérez, J. M., Starcevic, M., Gautam, R., and Dell'Angelica, E. C. (2002) BLOC-1, a novel complex containing the pallidin and Muted proteins involved in the biogenesis of melanosomes and platelet-dense granules. *J. Biol. Chem.* **277,** 28191–28199
12. Ilardi, J. M., Mochida, S., and Sheng, Z. H. (1999) Snapin: a SNARE-associated protein implicated in synaptic transmission. *Nat. Neurosci.* **2,** 119–124
13. Starcevic, M., and Dell'Angelica, E. C. (2004) Identification of Snapin and three novel proteins (BLOS1, BLOS2, and BLOS3/reduced pigmentation) as subunits of biogenesis of lysosome-related organelles complex-1 (BLOC-1). *J. Biol. Chem.* **279,** 28393–28401
14. Gwynn, B., Martina, J. A., Bonifacino, J. S., Sviderskaya, E. V., Lamoreux, M. L., Bennett, D. C., Moriyama, K., Huizing, M., Helip-Wooley, A., Gahl, W. A., Webb, L. S., Lambert, A. J., and Peters, L. L. (2004) Reduced pigmentation (*rp*), a mouse model of Hermansky-Pudlak syndrome, encodes a novel component of the BLOC-1 complex. *Blood* **104,** 3181–3189
15. Morgan, N. V., Pasha, S., Johnson, C. A., Ainsworth, J. R., Eady, R. A., Dawood, B., McKeown, C., Trembath, R. C., Wilde, J., Watson, S. P., and

Downloaded from www.jbc.org at National Institutes of Health Library, on July 12, 2012

Maher, E. R. (2006) A germ-line mutation in *BLOC1S3/reduced pigmentation* causes a novel variant of Hermansky-Pudlak syndrome (HPS8). *Am. J. Hum. Genet.* **78,** 160–166
16. Cullinane, A. R., Curry, J. A., Carmona-Rivera, C., Summers, C. G., Ciccone, C., Cardillo, N. D., Dorward, H., Hess, R. A., White, J. G., Adams, D., Huizing, M., and Gahl, W. A. (2011) A BLOC-1 mutation screen reveals that *PLDN* is mutated in Hermansky-Pudlak syndrome type 9. *Am. J. Hum. Genet.* **88,** 778–787
17. Straub, R. E., Jiang, Y., MacLean, C. J., Ma, Y., Webb, B. T., Myakishev, M. V., Harris-Kerr, C., Wormley, B., Sadek, H., Kadambi, B., Cesare, A. J., Gibberman, A., Wang, X., O'Neill, F. A., Walsh, D., and Kendler, K. S. (2002) Genetic variation in the 6p22.3 gene *DTNBP1*, the human ortholog of the mouse dysbindin gene, is associated with schizophrenia. *Am. J. Hum. Genet.* **71,** 337–348
18. Mullin, A. P., Gokhale, A., Larimore, J., and Faundez, V. (2011) Cell biology of the BLOC-1 complex subunit dysbindin, a schizophrenia susceptibility gene. *Mol. Neurobiol.* **44,** 53–64
19. Larimore, J., Tornieri, K., Ryder, P. V., Gokhale, Z., Zlatic, S. A., Craigie, B., Lee, J. D., Talbot, K., Pare, J. F., Smith, Y., and Faundez, V. (2011) The schizophrenia susceptibility factor dysbindin and its associated complex sort cargoes from cell bodies to the synapse. *Mol. Biol. Cell* **22,** 4854–4867
20. Di Pietro, S. M., Falcón-Pérez, J. M., Tenza, D., Setty, S. R., Marks, M. S., Raposo, G., and Dell'Angelica, E. C. (2006) BLOC-1 interacts with BLOC-2 and the AP-3 complex to facilitate protein trafficking on endosomes. *Mol. Biol. Cell* **17,** 4027–4038
21. Salazar, G., Craige, B., Styers, M. L., Newell-Litwa, K. A., Doucette, M. M., Wainer, B. H., Falcon-Perez, J. M., Dell'Angelica, E. C., Peden, A. A., Werner, E., and Faundez, V. (2006) BLOC-1 complex deficiency alters the targeting of adaptor protein complex-3 cargoes. *Mol. Biol. Cell* **17,** 4014–4026
22. Setty, S. R., Tenza, D., Truschel, S. T., Chou, E., Sviderskaya, E. V., Theos, A. C., Lamoreux, M. L., Di Pietro, S. M., Starcevic, M., Bennett, D. C., Dell'Angelica, E. C., Raposo, G., and Marks, M. S. (2007) BLOC-1 is required for cargo-specific sorting from vacuolar early endosomes toward lysosome-related organelles. *Mol. Biol. Cell* **18,** 768–780
23. Rodriguez-Fernandez, I. A., and Dell'Angelica, E. C. (2009) A data-mining approach to rank candidate protein-binding partners: the case of biogenesis of lysosome-related organelles complex-1 (BLOC-1). *J. Inherited Metab. Dis.* **32,** 190–203
24. Monfregola, J., Napolitano, G., D'Urso, M., Lappalainen, P., and Ursini, M. V. (2010) Functional characterization of Wiskott-Aldrich syndrome protein and scar homolog (WASH), a bi-modular nucleation-promoting factor able to interact with biogenesis of lysosome-related organelle subunit 2 (BLOS2) and γ-tubulin. *J. Biol. Chem.* **285,** 16951–16957
25. Hayes, M. J., Bryon, K., Satkurunathan, J., and Levine, T. P. (2011) Yeast homologs of three BLOC-1 subunits highlight K*x*DL proteins as conserved interactors of BLOC-1. *Traffic* **12,** 260–268
26. Hoover, D. M., and Lubkowski, J. (2002) DNAWorks: an automated method for designing oligonucleotides for PCR-based gene synthesis. *Nucleic Acids Res.* **30,** e43
27. Hierro, A., Kim, J., and Hurley, J. H. (2005) Polycistronic expression and purification of the ESCRT-II endosomal trafficking complex. *Methods Enzymol.* **403,** 322–332
28. Dell'Angelica, E. C., Ohno, H., Ooi, C. E., Rabinovich, E., Roche, K. W., and Bonifacino, J. S. (1997) AP-3: an adaptor-like protein complex with ubiquitous expression. *EMBO J.* **16,** 917–928
29. Dell'Angelica, E. C., Ooi, C. E., and Bonifacino, J. S. (1997) β3A-adaptin, a subunit of the adaptor-like complex AP-3. *J. Biol. Chem.* **272,** 15078–15084
30. Sheffield, P., Garrard, S., and Derewenda, Z. (1999) Overcoming expression and purification problems of RhoGDI using a family of "parallel" expression vectors. *Protein Expr. Purif.* **15,** 34–39
31. Lebowitz, J., Lewis, M. S., and Schuck, P. (2002) Modern analytical ultracentrifugation in protein science: a tutorial review. *Protein Sci.* **11,** 2067–2079
32. Cole, J. L., Lary, J. W., Moody, T. P., and Laue, T. M. (2008) Analytical ultracentrifugation: sedimentation velocity and sedimentation equilibrium. *Methods Cell Biol.* **84,** 143–179
33. Valentine, R. C., and Green, N. M. (1967) Electron microscopy of an antibody-hapten complex. *J. Mol. Biol.* **27,** 615–617
34. Heymann, J. B., and Belnap, D. M. (2007) Bsoft: image processing and molecular modeling for electron microscopy. *J. Struct. Biol.* **157,** 3–18
35. Shaikh, T. R., Gao, H., Baxter, W. T., Asturias, F. J., Boisset, N., Leith, A., and Frank, J. (2008) SPIDER image processing for single-particle reconstruction of biological macromolecules from electron micrographs. *Nat. Protoc.* **3,** 1941–1974
36. Penczek, P., Radermacher, M., and Frank, J. (1992) Three-dimensional reconstruction of single particles embedded in ice. *Ultramicroscopy* **40,** 33–53
37. Dell'Angelica, E. C., Aguilar, R. C., Wolins, N., Hazelwood, S., Gahl, W. A., and Bonifacino, J. S. (2000) Molecular characterization of the protein encoded by the Hermansky-Pudlak syndrome type 1 gene. *J. Biol. Chem.* **275,** 1300–1306
38. Sviderskaya, E. V., Hill, S. P., Evans-Whipp, T. J., Chin, L., Orlow, S. J., Easty, D. J., Cheong, S. C., Beach, D., DePinho, R. A., and Bennett, D. C. (2002) $p16^{Ink4a}$ in melanocyte senescence and differentiation. *J. Natl. Cancer Inst.* **94,** 446–454
39. Chaudhuri, R., Lindwasser, O. W., Smith, W. J., Hurley, J. H., and Bonifacino, J. S. (2007) Down-regulation of CD4 by human immunodeficiency virus type 1 Nef is dependent on clathrin and involves direct interaction of Nef with the AP-2 clathrin adaptor. *J. Virol.* **81,** 3877–3890
40. Wolf, E., Kim, P. S., and Berger, B. (1997) MultiCoil: a program for predicting two- and three-stranded coiled coils. *Protein Sci.* **6,** 1179–1189
41. Nazarian, R., Starcevic, M., Spencer, M. J., and Dell'Angelica, E. C. (2006) Reinvestigation of the dysbindin subunit of BLOC-1 (biogenesis of lysosome-related organelles complex-1) as a dystrobrevin-binding protein. *Biochem. J.* **395,** 587–598
42. Ren, Y., Yip, C. K., Tripathi, A., Huie, D., Jeffrey, P. D., Walz, T., and Hughson, F. M. (2009) A structure-based mechanism for vesicle capture by the multisubunit tethering complex Dsl1. *Cell* **139,** 1119–1129

Downloaded from www.jbc.org at National Institutes of Health Library, on July 12, 2012